Atmospheric Pollution Research 15 (2024) 102171

Contents lists available at ScienceDirect

Atmospheric Pollution Research

journal homepage: www.elsevier.com/locate/apr

Analyzing nitrogen dioxide to nitrogen oxide scaling factors for data-driven satellite-based emission estimation methods: A case study of Matimba/Medupi power stations in South Africa

Janne Hakkarainen [a,*], Gerrit Kuhlmann [b], Erik Koene [b], Diego Santaren [c], Sandro Meier [b,f], Maarten C. Krol [d,e], Bart J.H. van Stratum [d], Iolanda Ialongo [a], Frédéric Chevallier [c], Johanna Tamminen [a], Dominik Brunner [b], Grégoire Broquet [c]

[a] Finnish Meteorological Institute, Helsinki, Finland
[b] Swiss Federal Laboratories for Materials Science and Technology, Dübendorf, Switzerland
[c] Laboratoire des Sciences du Climat et de l'Environnement, Gif-sur-Yvette, France
[d] Wageningen University & Research, Wageningen, The Netherlands
[e] Utrecht University, Utrecht, The Netherlands
[f] Department of Geography, University of Zurich, Zurich, Switzerland

ARTICLE INFO

Dataset link: https://doi.org/10.5281/zenodo.7448143, https://data-portal.s5p-pal.com/

Keywords:
Nitrogen oxides
Nitrogen dioxide
Satellite data
Emission estimation
Plume inversion
Power station
MicroHH
Sentinel-5P
TROPOMI

ABSTRACT

In this paper, we propose improved nitrogen dioxide (NO_2) to nitrogen oxide (NO_x) scaling factors for several data-driven methods that are used for the estimation of NO_x power plant emissions from satellite observations of NO_2. The scaling factors are deduced from high-resolution simulations of power plant plumes with the MicroHH large-eddy simulation model with a simplified chemistry and then applied to Sentinel-5 Precursor (S5P) TROPOspheric Monitoring Instrument (TROPOMI) NO_2 satellite observations over the Matimba/Medupi power stations in South Africa. We show that due to the non-linear chemistry the optimal NO_2 to NO_x scaling factors depend on both the method employed and the specific segments of the plume from which emission estimate is derived. The scaling factors derived from the MicroHH simulations in this study are substantially (more than 50%) higher than the typical values used in the literature with actual NO_2 observations. The results highlight the challenge in appropriately accounting for the conversion from NO_2 to NO_x when estimating point source emissions from satellite NO_2 observations.

1. Introduction

Satellite observations of nitrogen dioxide (NO_2) in the troposphere have been available since the launch of Global Ozone Monitoring Experiment (GOME) in 1995. More recent satellite instruments, such as the Ozone Monitoring Instrument (OMI, Levelt et al., 2018), have been providing observations at much higher resolution allowing to better characterize signals from local anthropogenic sources (e.g., cities and power stations). Several different methods have been proposed to infer emissions of nitrogen oxide ($NO_x = NO_2 + NO$) from satellite NO_2 observations (e.g., de Foy et al., 2015; Beirle et al., 2011, 2019). As NO_x is often co-emitted with carbon dioxide (CO_2), space-based nitrogen dioxide (NO_2) observations have been used as indicators for fossil fuel combustion and CO_2 emissions at local scale (Reuter et al., 2014, 2019; Hakkarainen et al., 2021, 2023a). Furthermore, these observations have been used to study the effects of environmental policies and economic changes (e.g., Castellanos and Boersma, 2012; de Foy et al., 2016).

Nitrogen oxides are mostly (e.g., 95%) emitted in the form of nitrogen monoxide (NO), which is not observed by satellites. A typical assumption is that NO is quickly oxidized to NO_2 by reaction with ozone and the steady state NO:NO_2 ratio is reached within a few minutes (Seinfeld and Pandis, 2006). Often a constant NO_x:NO_2 ratio is assumed to infer the NO_x emissions from space-based NO_2 observations. Many studies (e.g., Beirle et al., 2011, 2019; de Foy and Schauer, 2022; Merlaud et al., 2020; Shaiganfar et al., 2017; Ionov et al., 2022; Potts et al., 2022; Hakkarainen et al., 2021) use the steady-state noontime molar concentration ratio under typical urban conditions of 1.32 based on Seinfeld and Pandis (2006). Recently, model-based concentration ratios have also been calculated using simulations from Copernicus Atmospheric Monitoring Service (CAMS, Lorente et al.,

* Corresponding author.
E-mail address: janne.hakkarainen@fmi.fi (J. Hakkarainen).

https://doi.org/10.1016/j.apr.2024.102171
Received 10 January 2024; Received in revised form 26 April 2024; Accepted 26 April 2024
Available online 29 April 2024

2019; Rey-Pommier et al., 2022) and Comprehensive Air Quality Model with Extensions (CAMx, Goldberg et al., 2022). Beirle et al. (2021) calculated NO_x:NO_2 ratios according to the photo-stationary steady state. In general, these studies show small deviations from the value 1.32 (e.g., 1.16–1.83), but acknowledge that values near the point sources are likely to be higher. CHIMERE model simulations (Shaiganfar et al., 2017) further indicate that in large circles around Paris, the partitioning ratios are smaller during summer (1.32) than in winter (1.51), due to the higher ozone mixing ratios in summer. In contrast to model-based analyses, the Dutch aircraft measurements of in-plume NO_x/NO_2 ratios from power stations (e.g., Janssen, 1988; Vilà-Guerau de Arellano et al., 1990; Bange et al., 1991; Hanrahan, 1999) often showed values higher than 10 near the source and values between 2 and 10 up to 15 km from the source.

Two classes of data-driven approaches have been used to infer local NO_x emissions from satellites. The first approach is based on averaging NO_2 satellite data over long periods of time and the second is based on inferring emissions from instantaneous NO_2 observations. In both cases the emission estimates are related to the local satellite overpass time. Both methods do not integrate full chemistry models but use simple assumptions to account for the NO_2 lifetime and the conversion from NO_2-derived emissions to NO_x emissions. With the previous generation of NO_2 observing satellites (e.g., OMI), averaging (via oversampling) was often necessary to improve the precision and the spatial resolution (Beirle et al., 2011). Emission estimation methods based on the analysis of individual emission plumes have been mostly applied to long-lived greenhouse gases such as CO_2 and methane (CH_4), which do not require adjustment due to the lifetime (Varon et al., 2019). Since the launch of the TROPOspheric Monitoring Instrument (TROPOMI) on board the Copernicus Sentinel-5 Precursor (S5P) satellite in 2017, it has been possible to derive NO_x emissions from anthropogenic sources based on NO_2 observations from individual orbits (e.g., Lorente et al., 2019; Rey-Pommier et al., 2022; Zhang et al., 2023), thanks to the improved spatial resolution (currently 5.5 km by 3.5 km at nadir for NO_2).

In this paper, we analyze NO and NO_2 plumes originating from the Matimba/Medupi power stations in South Africa based on high resolution NO_x simulations and real NO_2 satellite data. We apply four NO_x emission estimation methods based on instantaneous NO_2 scenes and two methods that infer NO_x emissions from averaged NO_2 data. We use MicroHH (van Heerwaarden et al., 2017) large-eddy simulations (LES) with condensed and efficient plume chemistry to study the optimal NO_2 to NO_x scaling factor f for each emission estimation method. Furthermore, we use S5P/TROPOMI NO_2 observations to infer the NO_x emissions and analyze the sensitivity of the results to the assumptions made regarding the NO_2 to NO_x scaling factor. We compare the emission estimates to the reported information.

2. Materials and methods

2.1. Matimba/Medupi power stations

We analyze the NO_x emission estimates from the Matimba and Medupi coal-fired power stations previously studied by Hakkarainen et al. (2021). These two power stations operated by Eskom are located about 6 km apart in the Highveld region in South Africa (23.67°S, 27.61°E) and are isolated from other strong emission sources in the region. Eskom reports total monthly NO_x emissions (using standards BS EN 14181:2004 - Quality Assurance of Automated Measuring Systems and ESKOM internal standard 240-56242363 Emissions Monitoring and Reporting) as well as daily energy production (see https://www.eskom.co.za/dataportal/emissions/ael/ for monthly reports and more details). We disaggregate the reported monthly emissions to daily emissions based on the daily energy consumption (as a fraction of total monthly energy consumption). The daily and monthly emissions for the year 2021 are given in Fig. 1. The total annual NO_x emission of the two power stations is 101 ± 12 kton/year. As usual, NO_x emissions are reported in terms of NO_2 equivalent.

2.2. MicroHH model

To calculate method-dependent NO_2 to NO_x scaling factors, we use the MicroHH (van Heerwaarden et al., 2017) large-eddy simulations (LES) generated for the Matimba power station within the H2020 project CoCO2 (see Krol et al., 2024, for more details). The simulation period is 48 hours starting from 24 July 2020 00 UTC. Following the CoCO2 simulation protocol, based on the Community Emissions Data System (CEMS) for the year 2014, the simulation uses constant NO_x emission of 1.9676 kg s^{-1} (62 kton/year, in terms of NO_2 equivalent) of which 95% is NO and 5% is NO_2.

The MicroHH LES simulations were initialized and driven by ERA5 (meteorology) and CAMS (non-reactive and reactive gases), with a coupling as described by Neggers et al. (2012) and van Stratum et al. (2023). The horizontal resolution was 100 m×100 m and the vertical resolution 25 m. The chemistry scheme is a condensed version of the scheme implemented in the European Centre for Medium-Range Weather Forecasts (ECMWF) Integrated Forecasting System (IFS, Huijnen et al., 2016) and focuses on correct calculations of the equilibrium between NO_x and ozone (photo-stationary state) and NO_x lifetime. Photolysis rates are calculated at 500 m above the surface for clear sky conditions with the TUV module (Madronich and Flocke, 1999). The simulated species are: HNO_3, NO_3, N_2O_5, H_2O_2, CO, HCHO, ROOH, C_3H_6 (generic hydrocarbon), RO_2, HO_2, NO, NO_2, OH (and fixed CH_4 and H_2). The Rosenbrock solver of the kinetic rate equations was generated automatically by the Kinetic Pre Processor (KPP, Damian et al., 2002; Sandu et al., 2022).

The chemistry used in the MicroHH model (Krol et al., 2024) is simplified, and does not contain PAN and alkyl-nitrates. However, the model has been calibrated against a more complex chemistry implemented in the IFS. This version, which includes PAN and alkyl-nitrates, is used for the CAMS reanalysis (Inness et al., 2019) and serves as chemical boundary conditions for the MicroHH simulations. The simplified chemistry introduces additional uncertainty, but the main chemical processes that determine the NO_x/NO_2 ratio and NO_2 lifetime are adequately modeled. MicroHH is one of the few Large Eddy Simulation models that resolves atmospheric chemistry (Krol et al., 2024). Plume dispersion in MicroHH was tested and evaluated against wind tunnel experiments in Razňjević (2023).

For the practical calculation we use the "Library of Plumes" dataset created in the H2020 project CoCO2 (Koene and Brunner, 2022, 2023). In the dataset, the vertical column densities (VCD) of NO, NO_2 and CO_2 are available with hourly resolution on a 2 km×2 km grid to mimic the upcoming CO2M satellite (Meijer et al., 2020).

2.3. S5P/TROPOMI NO_2 observations

The TROPOspheric Monitoring Instrument (Veefkind et al., 2012) was launched onboard the Copernicus Sentinel-5P satellite on 13 October 2017. The satellite has an equatorial crossing time of 13:30 LT. The current spatial resolution is 5.5 km by 3.5 km at nadir and covers a swath of about 2600 km wide. Here we use the tropospheric NO_2 vertical columns with quality flag qa_value ≥ 0.75 and the effective cloud fraction ≤ 0.3. Due to changes in the operational algorithm, we use the version v02.03.01 intermediate reprocessing on the S5P-PAL system https://data-portal.s5p-pal.com/, which provides a seamless connection with the operational version 2.3.1 data product. Technical details can be found from the readme file: https://data-portal.s5p-pal.com/product-docs/no2/PAL_reprocessing_NO2_v02.03.01_20211215.pdf.

We use the TROPOMI NO_2 observations from the year 2021 to estimate the NO_x emission from Matimba/Medupi power stations. The S5P/TROPOMI overpass time is around 12 UTC over these stations. Following Beirle et al. (2019), we recalculate the air mass factors using NO_2 profiles representative for the emission plume. Based on the MicroHH simulations, the NO_2 inside the plume is rapidly mixed with background air in the planetary boundary layer with a mean

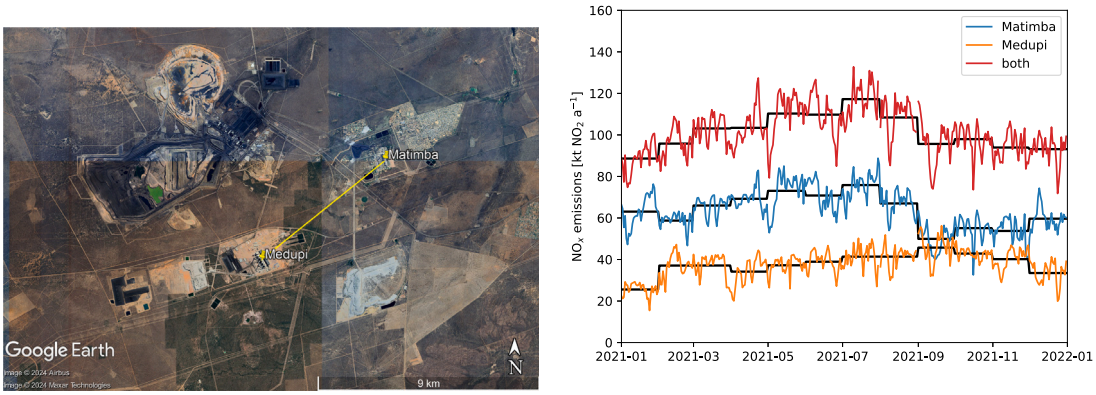

Fig. 1. (left) Matimba and Medupi power stations in South Africa about 6 km apart. (right) Monthly NO_x emissions converted to daily emissions using power generation reported by Eskom. Black lines indicate monthly emissions.

mole fraction of about 5 nmol mol^{-1}. We therefore recomputed AMFs by updating NO_2 profiles inside the PBL height from ERA-5, which results in a multiplicative correction factor of 1.27 for TROPOMI NO_2 columns inside the plume. This value is in good agreement with the AMF correction factor of 1.35 found by Beirle et al. (2019) for South Africa.

2.4. NO_x emission estimation methods

We use six emission estimation methods of which four (integrated mass enhancement, Gaussian plume, cross-sectional flux and light cross-sectional flux methods) are based on the analysis of instantaneous observations and two (exponentially modified Gaussian and divergence methods) are based on temporally averaged data. All the methods estimate the emission corresponding to the local TROPOMI overpass time. These computationally light methods were selected based on a benchmark analysis (Santaren et al., 2024) carried out in the H2020 project CoCO2 (Hakkarainen et al., 2023b) and are included in the *ddeq* Python library for data-driven emission quantification of hotspots. Kuhlmann et al. (2024) gives a comprehensive description of the *ddeq* implementation. The methods used in the analysis are briefly summarized below:

- In the Gaussian plume (GP) model method, the emission E is derived by fitting a 2D Gaussian plume function to the observations (e.g. Bovensmann et al., 2010; Nassar et al., 2017):

$$G(x,y) = \frac{E}{\sqrt{2\pi}\sigma(x)U} e^{-\frac{y^2}{2\sigma^2(x)}} \tag{1}$$

  where U is the effective wind speed and $\sigma = \sqrt{2Kx^b/U}$ is the standard width depending on the eddy diffusion coefficient K and an additional exponential parameter b. With short-lived gases, an exponential decay that multiplies $G(x,y)$ is also fitted:

$$D(x,\tau) = \exp\left(-\frac{x}{U\tau}\right) \tag{2}$$

  where τ is the exponential decay time. Furthermore, our implementation allows the Gaussian plume to be curved.
- For the cross-sectional flux methods, we use two different implementations: the cross-sectional flux (CSF) method described by Kuhlmann et al. (2020, 2021) and the light cross-sectional flux (LCSF) originally developed by Zheng et al. (2020) and Chevallier et al. (2022) for OCO-2 and adapted for TROPOMI in the CoCO2 project. In both versions, the emission is derived from the integrals of the cross-section of the plume perpendicular to the wind direction (i.e. line density) multiplied with the effective wind speed U. Gaussian curves are fitted for calculating the line densities (e.g., Reuter et al., 2019) to better constrain noisy observations and to interpolate (possibly) missing data. The LCSF implementation uses information closer to the source (one hour downwind), whereas the CSF method analyzes the full detectable plume using sub-polygons every 5 km downwind of the source. The LCSF method assumes a NO_x and NO_2 lifetime of 4 hours, while the CSF method computes the NO_x decay time as an additional fit parameter.
- The integrated mass enhancement (IME) method calculates the emission from the total plume mass above the background. Following the approach by Frankenberg et al. (2016), for inert gases like CO_2 and CH_4, the emission can be calculated as $E = U \times \mathrm{IME}/L$, where U is the wind speed, IME is the integrated mass enhancement (above the background) and L is the distance from the source up to where the plume is integrated. For NO_x, a correction factor c can be derived from a Gaussian plume model multiplied with an exponential decay:

$$E = \frac{1}{c}\frac{U}{L}\mathrm{IME} \quad \text{with} \quad c = \frac{U\tau}{L}\left(1 - \exp\left(-\frac{L}{U\tau}\right)\right). \tag{3}$$

  Here, τ is the NO_x lifetime, which is assumed to be 4 hours (see Kuhlmann et al., 2024, for details).
- In the exponentially modified Gaussian (EMG) method, the emission is calculated from the averaged data. Here, the data is rotated according to the wind direction so that all scenes have wind direction from west to east. The resulting rotated mean field is then integrated along the latitudinal dimension to derive the NO_2 line densities. The emission E is obtained by fitting the averaged line densities with the EMG model $M(x)$ (as in Beirle et al., 2011; de Foy et al., 2014) as follows:

$$M(x) = \frac{E}{U} \times (e * G)(x) + B. \tag{4}$$

  Here $(e * G)(x)$ is the convolution between the exponential decay and the Gaussian function, and B is the background.
- The divergence (DIV) method is based on calculating the divergence D of the averaged fluxes that are derived from the vertical column densities and the wind components. The emission field E is obtained from the divergence D according to the continuity equation for steady state, $D = E - S$, where S indicates the sink term. The emissions from point sources are obtained from the emission field by using the Gaussian peak fitting approach (Beirle et al., 2019, 2021). The version used here is described in Hakkarainen et al. (2022). First, the fluxes are calculated using the tropospheric NO_2 columns and effective wind speed. The divergence D is calculated from the averaged fluxes. The sinks are calculated as $S = V/\tau$, where V is the mean vertical column density and τ the assumed lifetime. The emissions fields are calculated as $E = D + S$ and fitted with the Gaussian peak fitting function.

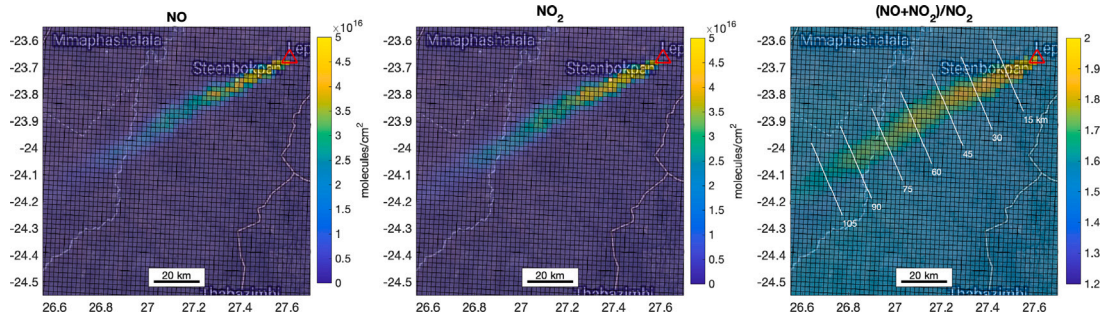

Fig. 2. MicroHH simulations of NO and NO_2 columns and the NO_x:NO_2 molar concentration ratio. The maximum value is 8.7 in the grid cell closest to the Matimba power station marked with red triangle. The background value is about 1.5. White lines perpendicular to the plume indicate transects at different distance from the source (red triangle). The spatial resolution of the data is 2 km × 2 km.

The methods based on instantaneous images also require plume detection, background extraction and center line fitting. Here we use the plume detection described by Kuhlmann et al. (2021), which has the following four steps: (1) pixels significantly enhanced above the background are detected based on a statistical test; (2) detected pixels are grouped into regions (plumes); (3) a region of connected enhanced pixels is assigned to a point source; and (4) a centerline is fitted to the detected pixels for each plume as a two-dimensional curve. The algorithm is used by the GP, CSF and IME method. However, the LCSF methods identifies the centers and width of plume transects fitting a Gaussian function to the NO_2 enhancements in the across-wind direction, close and downwind to the source, using the wind direction provided by the model.

For the GP, CSF and IME method, the background is computed by masking the detected plume and applying a normalized convolution, while the LCSF method computes the background by fitting a linear term in addition to the Gaussian function to the NO_2 concentrations in the across-wind direction.

The NO_x emission estimates are calculated from satellite-based NO_2 observations. We use a scaling factor f, to convert NO_2-derived emissions to NO_x emissions, i.e., $E_{NO_x} = f \times E_{NO_2}$. We note that the widely used scaling factor 1.32 is a molar ratio and therefore E_{NO_x} corresponds to the emission reported as NO_2 equivalents. Here we derive the method-specific scaling factors as $f = E_{NO_x}/E_{NO_2}$, where E_{NO_x} and E_{NO_2} are the emissions calculated from the NO_x and NO_2 MicroHH LES simulations, respectively.

3. Results

3.1. Analysis of MicroHH simulations

Fig. 2 shows an example of NO and NO_2 vertical column densities from MicroHH large-eddy simulations (25 July 2020 12:00 UTC). As expected, the NO_x:NO_2 molar concentration ratio is higher near the emission source, where values higher than 2 are observed until about 20 km downwind from the source. The maximum value is 8.7 in the grid cell closest to the source. In this case, the background ratio is about 1.5, which is in the typical range (e.g., Fig. 2 in Beirle et al., 2023), but slightly higher than 1.32. Due to chemistry, the molar concentration ratios are exponentially decreasing along the plume.

We use the MicroHH simulations to derive the emissions from the NO_x VCDs (NO + NO_2) and from the NO_2 VCDs only. The latter option is the only one available with real satellite observations. The NO_2 to NO_x scaling factors for each method are inferred from the mean emissions as $f = E_{NO_x}/E_{NO_2}$.

Fig. 3 shows the time series of the estimated NO_x emissions using the LCSF, CSF, GP, and IME methods. Overall, across all the methods, the mean NO_x emissions (solid lines in Fig. 3) are in good agreement with the emission value used in the simulation (dashed lines in Fig. 3). Here, and throughout the rest of the manuscript we express NO_x emission as NO_2 equivalents. In the case of chemically inactive species like CO_2, the emissions from each method are also very close to the emission value used in the simulation (see supplementary file, Figs. S1–S4). The NO_2-derived emissions are multiplied with a scaling factor f computed as the ratio of the mean NO_x and NO_2 emission estimates. The uncertainty was estimated from the standard deviation of the ratios. The estimated mean scaling factors $f = E_{NO_x}/E_{NO_2}$ are 1.71 ± 0.29, 2.73 ± 0.64, 2.17 ± 0.48 and 1.83 ± 0.58 for the IME, GP, CSF and LCSF methods, respectively. These values are significantly higher than the values typically used in the literature (e.g., 1.32). The scaling factors f for each method are dependent on the part of the plume used for emission calculation, as discussed below. The daytime (9–15 UTC) scaling factors f_d are about 3%–10% larger (except for GP method 13% smaller), with the mean values of 1.83, 2.38, 2.24 and 2.02 for the corresponding methods. The daytime standard deviation is about 0.2 to 0.3 for all the methods.

The optimal scaling factor depends on the plume length used in the calculation as shown for the IME approach in Fig. 4. The factor is about 3.7 for a 15 km long plume and drops rapidly reaching values smaller than 1.7 for 50 km long plumes. Note that the scaling factor for the IME method is independent of the assumed decay time that impacts NO_2 and NO_x in the same way.

The scaling factor can be used to understand where a method obtains information about the emissions. The IME method uses all measurements up to 50 km downwind of the source. Likewise, the LCSF method uses only measurements one hour downwind of the source, which ranges between 13 and 42 km depending on wind speed. Consequently, the LCSF method has a larger scaling factor than the IME method. The GP method has the highest scaling factor of 2.73 implying that it mostly uses VCDs at distances below 30 km where the signal-to-noise ratio is largest. In contrast, the CSF method computes fluxes at several distances downwind from which the emission rate and decay time are estimated, which apparently gives a higher weight to downwind values.

The decay time for the NO_x columns was estimated as an additional fit parameter in the Gaussian plume and cross-sectional flux inversion methods (Figs. S2 and S3). The corresponding median values of 2.8 and 6.6 hours are consistent with the typical value of 4 hours used in previous studies and assumed here for the IME and LCSF methods. For the NO_2 columns, the estimated decay times are higher (9.0 h and 13.5 for GP and CSF method) than for NO_x. This is likely caused by the increase of NO_2 columns downwind from the source due to the conversion of NO to NO_2. We note that lifetimes reported here are effective decay times, and in general, the lifetime as mass/loss is not constant along the plume.

The analyzed MicroHH simulation is 48 hours long. For the methods that use averaged data for emission estimation (EMG and divergence method), calculating the emissions from a 2 day simulation is challenging. Fig. 5 shows the line densities of the rotated data and the EMG fits for both NO_x and NO_2 emission estimation. By comparing

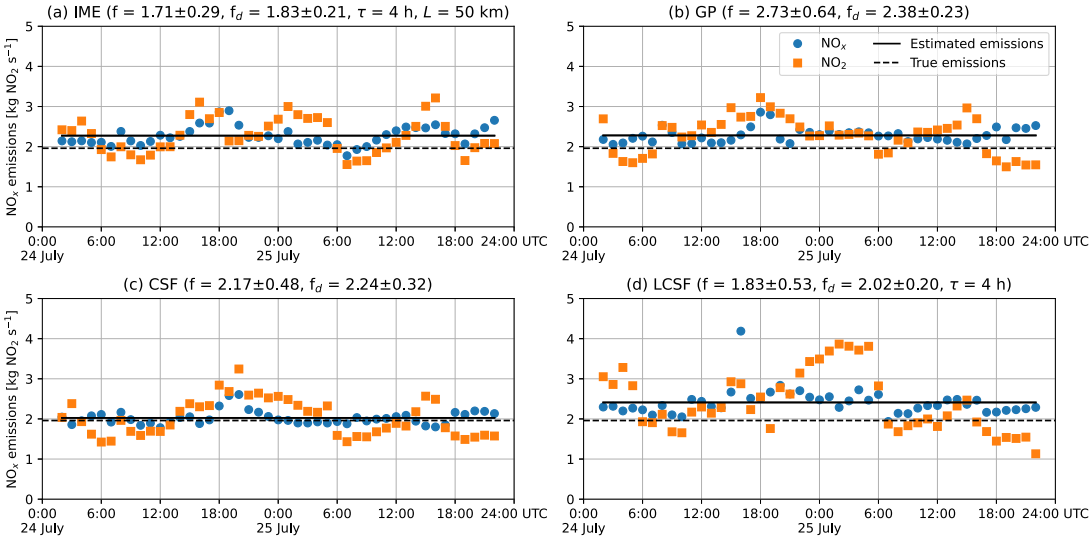

Fig. 3. Time series of estimated NO_x emissions from MicroHH simulations using (a) IME, (b) GP, (c) CSF and (d) LCSF method. Emissions were estimated from NO_2 and NO_x observations. The NO_2-derived emissions were multiplied with a method-specific scaling factor f. In addition, the scaling factor f_d was computed using only daytime data (9–15 UTC). The uncertainty was estimated from the standard deviation of the ratios. IME and LCSF assume a fixed decay time of four hours.

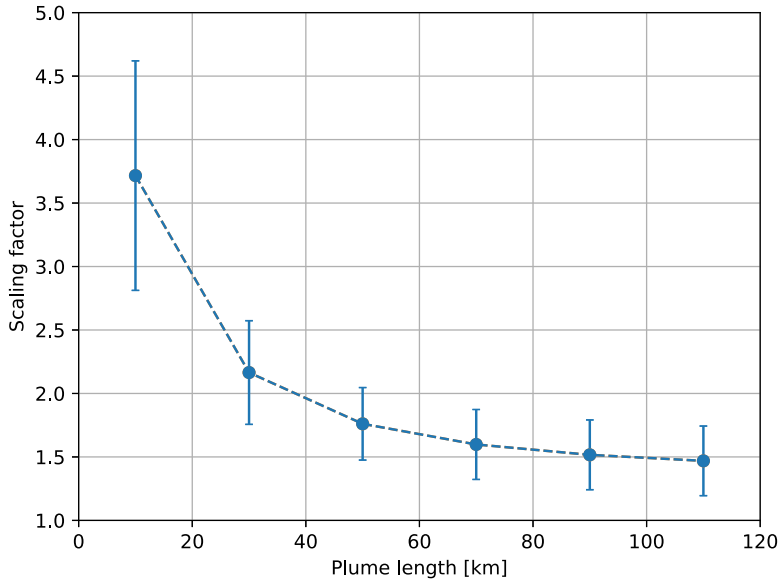

Fig. 4. Dependency of the scaling factor on plume length estimated from the IME method.

the emission estimates derived from the respective EMG fits, we obtain $f = 2.14 \pm 0.10$. We note that the NO_2 peak is located further away from the source (as compared to NO_x) due to the conversion from NO to NO_2. The photo-stationary state equilibrium under these conditions is reached only after about 1 h. The lifetime estimated by the EMG fit is 1.5 times higher for NO_2 than for NO_x (3.1 h vs 2.1 h). Moreover, the lifetimes are not constant along the plume. As discussed in more detail in Krol et al. (2024), the plume lifetime is determined both by mixing (entrainment of background ozone into the plume) and the strength of the NO_x emissions. When emissions are large, as in the Matimba case, the plume stays chemically intact longer, because the emitted NO (95% of NO_x) efficiently titrates the entrained ozone.

Fig. 5 (inset) also shows the molar ratio of NO_x and NO_2 line densities. Ratios of about 3.2 are found near the source and are rapidly decreasing to about 1.5 after 20 km. This also indicates that the methods that use information closer to the source need a higher scaling factor. We were not able to calculate the NO_2 to NO_x scaling factor for the divergence method, but the peak fitting approach included in this method primarily uses information close to the source as well. In this case, we would need a longer simulation and data across all wind directions to successfully apply the peak fitting approach.

Finally, we note that all the methods (GP, CSF and EMG) that estimate the exponential decay time τ from the observations give higher scaling factors than the methods (IME and LCSF) that assume fixed NO_x and NO_2 decay time of four hours (2.38, 2.24 and 2.14 vs. 1.83 and 2.02). Part of the reason is that estimated decay times for NO_x are significantly lower (30%–70%) than the decay times obtained from the NO_2 observations, because the estimated NO_2 lifetime compensates for the conversion of NO to NO_2, which increases the apparent lifetime of NO_2. In general, lower estimated lifetimes correspond to higher emissions, which results in higher scaling factors as $f = E_{NO_x}/E_{NO_2}$. In particular, here the LCSF method gives a lower scaling factor than the CSF method, which would be unexpected (as LCSF uses information closer to the emission source) without considering the fact that with the CSF method the estimated decay times for NO_x are about 50% lower than for NO_2.

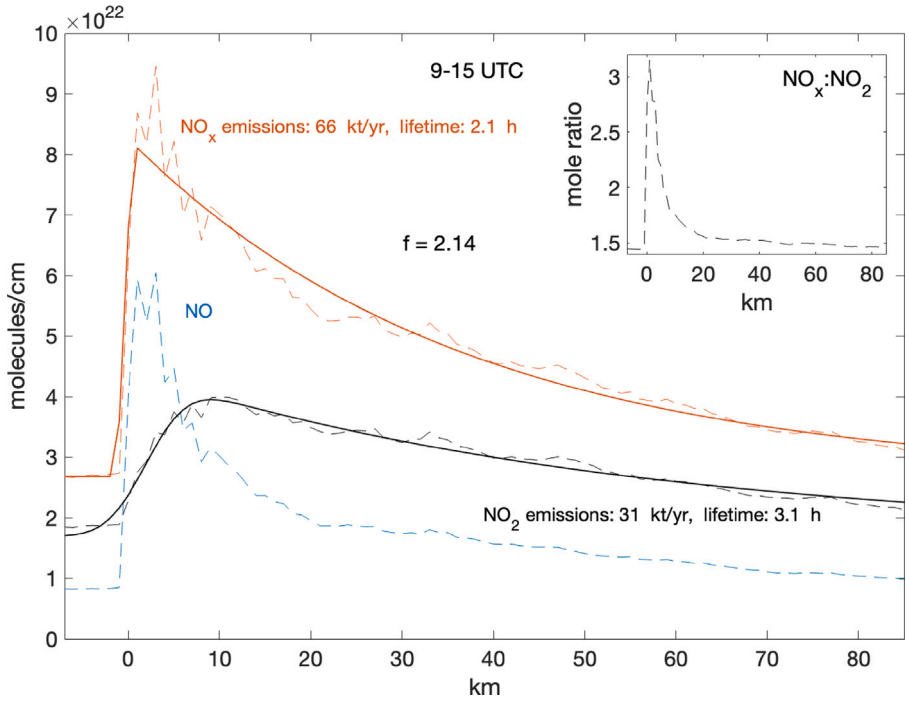

Fig. 5. MicroHH NO_x (red), NO (blue) and NO_2 (black) line densities (dashed lines) as a function of distance from the source. The solid lines are fits from the EMG model. The inset shows the molar ratio of NO_x and NO_2 line densities.

3.2. Results with S5P/TROPOMI data

Fig. 6 illustrates an example of an individual NO_2 plume emitted by the Matimba/Medupi power plants as observed by S5P/TROPOMI on 25 July 2021. As the distance between the power stations is only 6 km, they appear as a single source. The NO_x emission estimates based on the IME, GP, CSF and LCSF methods range between 78 kton/year and 99 kton/year, which is lower than the reported emission values of 130 kton/year. These estimates are derived by already applying the larger method-dependent NO_2 to NO_x scaling factors f obtained from the MicroHH analysis and the AMF-related correction factor of 1.27. For all methods, we use the vertically averaged ERA5 winds based on a typical emission profile used in simulations as presented by Brunner et al. (2019). For the CSF and GP methods, the lifetimes are fitted from the observations. For the IME and LCSF methods, which do not provide an estimate of the lifetime, we assume a constant NO_x lifetime of 4 h.

Fig. 7 shows the NO_x emissions estimation time series based on the four methods compared to the reported Matimba/Medupi NO_x emissions. All methods, especially IME and CSF, show higher emission estimates during the austral winter months. During the austral summer, we generally obtain values lower than reported. The temporal variability is also quite large compared to the reported NO_x variability. There are also large differences between the methods in terms of temporal evolution and scatter. One must note that the scaling factors f were derived from 48h-LES simulations during austral winter (July 2020) and might not be representative of the conditions during the rest of the year (e.g., Shaiganfar et al., 2017).

Next, we analyze the Matimba/Medupi NO_x emissions based on the methods using temporal averaging. Fig. 8 shows the NO_2 line densities and the fit derived using the EMG approach. We obtain a lifetime of 3.5 hours and a NO_x emission of 80 kton/year assuming a NO_2 to NO_x scaling factor of 1.32. Considering the AMF-related correction factor of 1.27 used here, the emission estimate of 80 kton/year is in agreement with those NO_x emissions of about 60 kton/year reported in recent studies (Hakkarainen et al., 2021; Potts et al., 2022) that also used the EMG method, but were applied to different TROPOMI NO_2 data versions and time periods.

Fig. 9 shows the results using the divergence method. The first panel shows the sinks calculated using the assumed lifetime of four hours, the second panel is the divergence, and the third panel is the emissions, i.e., $E = S + D$. Like for the EMG method, we use a NO_2 to NO_x scaling factor of 1.32. The emissions from the Matimba/Medupi power stations are clearly visible and easy to fit. When a peak function is fitted to the average emission map (third panel), we obtain the NO_x emissions of 52 kton/year. This is comparable to previous studies: Beirle et al. (2021) obtained emissions of 21 kton/year, whereas Beirle et al. (2019) obtained emissions of 54 kton/year (after applying correction for different factors such as AMF, lifetime, and winds, see Beirle et al. (2021) for more details). Beirle et al. (2023) obtained NO_x emissions of 76 kton/year for the year 2021 with a significantly updated method.

Fig. 10 summarizes the annual emission estimates using the different methods. The emissions are presented using the scaling factor 1.32 (dark colors) as well as with the method-dependent scaling factors (light colors). With the scaling factor 1.32, all the methods systematically underestimate the reported Matimba/Medupi annual NO_x emissions of about 100 kton/year. With the method-based scaling factors, the annual emissions are substantially closer to the reported emissions. Assuming that the reported values are correct and with the right temporal representation, these results indicate that method-specific scaling factors are needed to better calculate the true NO_x emissions for strong point sources like the Matimba/Medupi power station. As the MicroHH simulation was only 48 hours long, we could not calculate a specific scaling factor for the divergence method. To obtain NO_x emission values with the divergence method compatible with the reported emissions, we would need a NO_2 to NO_x scaling factor of about 2.5. This value is plausible as the emissions are inferred via peak fitting above the source. In this case, the standard deviations of the 2D Gaussian peak function were 7 km and 5 km in x and y directions, respectively.

4. Discussion and conclusions

In this paper, we analyzed optimal NO_2 to NO_x scaling factors for several data-driven satellite-based emission estimation methods. The

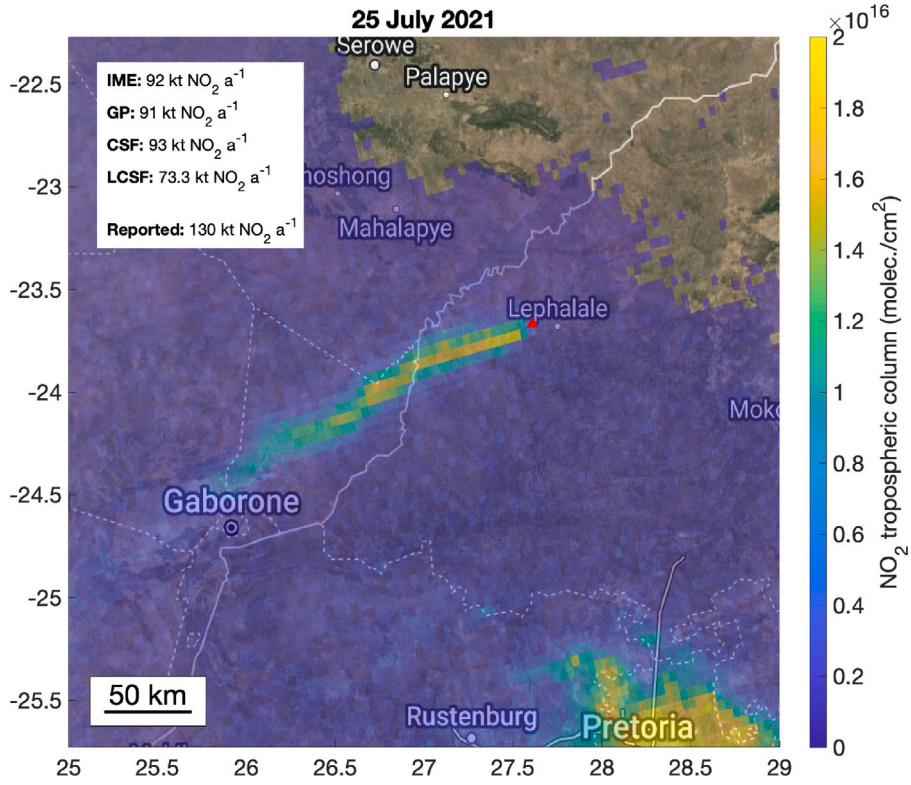

Fig. 6. Sentinel-5P/TROPOMI NO_2 plume from Matimba/Medupi (red triangle) observed on 25 July 2021 (on © Google Maps 2023 background). The NO_x emission estimates obtained with the IME, GP, CSF, and LCSF methods as well as the reported emissions are shown in the top left.

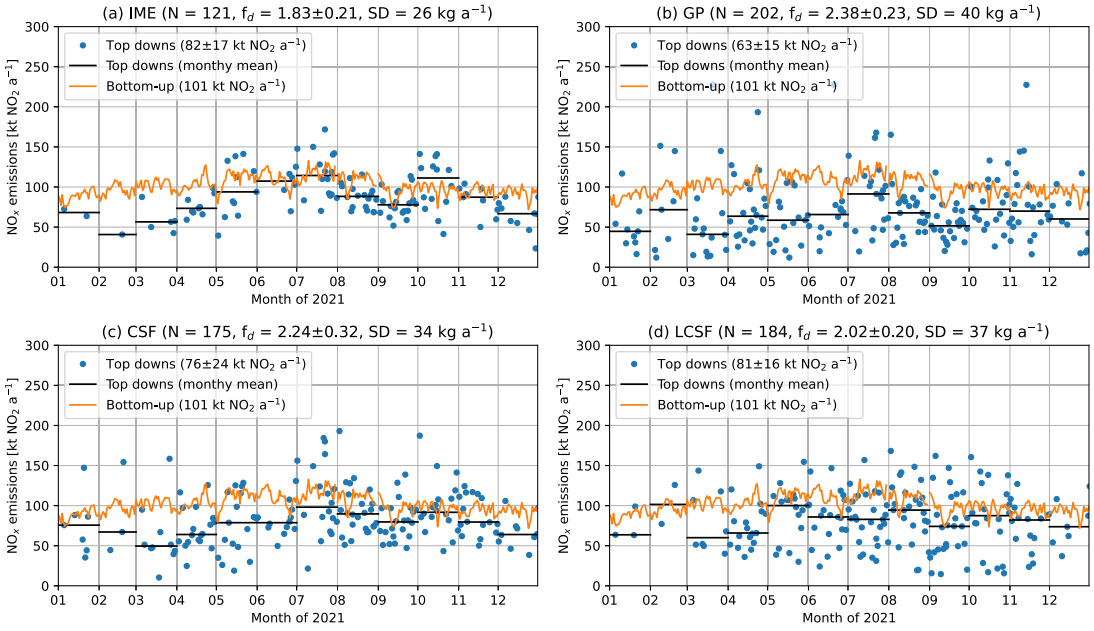

Fig. 7. Time series of the NO_x emission estimates obtained with the (a) IME, (b) GP, (c) CSF, and (d) LCSF method with monthly means. The emission estimates are compared against Eskom-reported emissions. The title shows the number of estimates N, the used scaling factor f_d and the scatter between top-down and bottom-up emission estimates.

results based on the MicroHH simulations show that the optimal scaling factors depend on the selected method because the different methods exploit information from different down-wind distances of the plume. In general, the scaling factors are higher if the information comes from near the point source and smaller if larger spatial areas are considered. This is because the NO_x/NO_2 concentration ratios vary strongly within the plume, with the highest values at the source pixel, while the values downwind are closer to literature values. Depending on the method, the scaling factors vary between 1.8 and 2.4, which is substantially higher than the values typically used in the literature in the case of Matimba/Medupi power plants. Aircraft measurements of plume NO_x/NO_2 ratios (e.g., Janssen, 1988; Vilà-Guerau de Arellano et al., 1990; Bange et al., 1991; Hanrahan, 1999) also indicate much higher values near the source. These higher scaling factors could partly explain why some studies (e.g., Beirle et al., 2021) have reported too low NO_x emission estimates. Also, the three-dimensional radiative transfer effects, reported

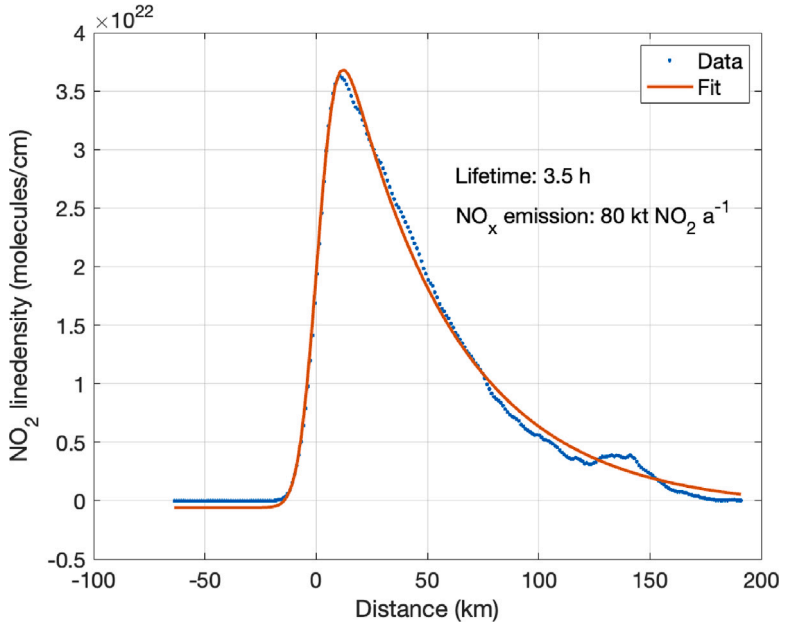

Fig. 8. Illustration of the exponentially modified Gaussian (EMG) method applied to the Matimba/Medupi power stations for 2021 based on Sentinel-5P/TROPOMI NO_2 observations using f = 1.32.

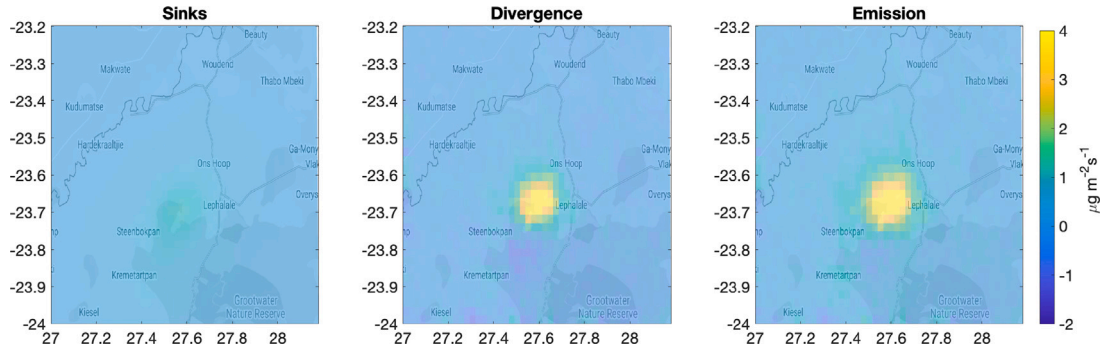

Fig. 9. Illustration of the divergence method for Matimba/Medupi power stations in 2021 based on Sentinel-5P/TROPOMI NO_2 observations.

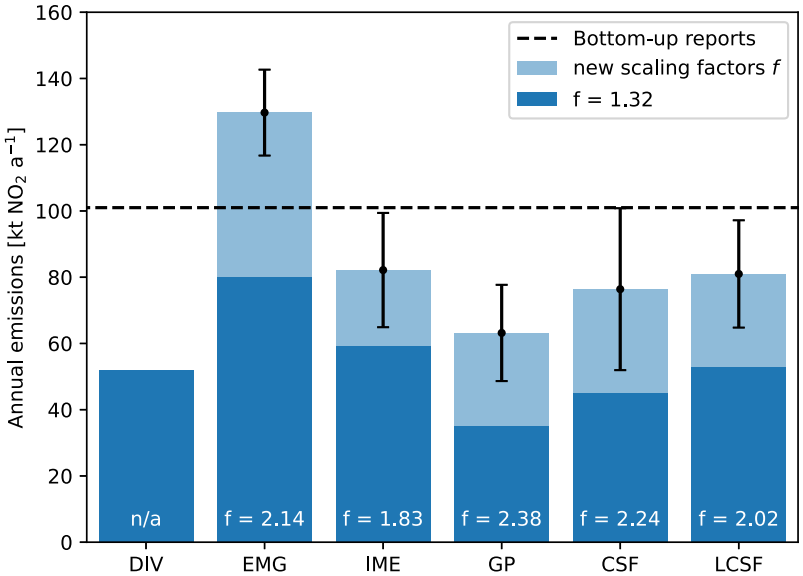

Fig. 10. Summary of the annual NO_x emission estimates for Matimba and Medupi power stations using method-dependent scaling factors (f_d, light colors) and f = 1.32 (dark colors). The error bars show variability (1σ) of the scaling factor. Other sources of uncertainty are not included in the error bar.

by Schwaerzel et al. (2020) and Wagner et al. (2023), can lead to underestimation of the true trace gas content. Here, we further verify that emission estimates obtained with method-specific scaling factors derived from a small set of MicroHH simulations are closer to the reported emissions in the Matimba/Medupi power station case study. The optimal scaling factors are likely not constant for a given method but additionally depend on the strength of the emission source, the meteorological conditions, background ozone concentration levels, and NO_x lifetime. In general, the scaling factors are expected to be smaller during summer than in winter, due to the higher ozone mixing ratios in summer (e.g., Shaiganfar et al., 2017). We note that if the emission values used for the MicroHH simulations are substantially overestimated or underestimated the scaling factors could be overestimated or underestimated, respectively, due to the changes in the $NO–NO_2–O_3$ chemistry and hence the partitioning between NO and NO_2. When emissions are large the plume stays chemically intact longer (Krol et al., 2024). The method-dependent scaling factors obtained here should thus not be interpreted as being universally applicable for the respective method.

We used a specific 48 hour MicroHH large-eddy simulation to calculate optimal NO_2 to NO_x scaling factors for the Matimba/Medupi power station. In general, calculating optimal scaling factors from large-eddy simulations can only be a partial solution when data-driven and computationally light emission inversion methods are used. High resolution model simulations with NO_x chemistry for each source and time period can be computationally expensive as the MicroHH simulations here. However, more comprehensive simulations with systematic variation of all influencing factors could potentially lead to a formulation of method-specific scaling factors as a function of these factors. The methods that are based on data averaging, the divergence method in particular, would optimally need one year of simulations for each source.

The method-specific NO_2 to NO_x scaling factors are needed as only NO_2 is observed from satellites. Another option could be to convert NO_2 columns to NO_x columns using spatially explicit maps of molar concentration ratio and then use these fields to infer emissions without scaling factors. The explicit concentrations maps could be generated for small sets of plumes with high-resolution modeling, and in larger studies parametric solutions could be used. These options are left for future studies. All in all, the results presented here highlight the need to appropriately account for the conversion from NO_2 to NO_x.

CRediT authorship contribution statement

Janne Hakkarainen: Conceptualization, Formal analysis, Investigation, Methodology, Writing – original draft, Writing – review & editing. **Gerrit Kuhlmann:** Conceptualization, Formal analysis, Investigation, Methodology, Writing – original draft, Writing – review & editing. **Erik Koene:** Data curation, Formal analysis, Investigation, Methodology, Writing – review & editing. **Diego Santaren:** Formal analysis, Investigation, Methodology, Writing – review & editing. **Sandro Meier:** Formal analysis, Writing – review & editing. **Maarten C. Krol:** Data curation, Formal analysis, Investigation, Methodology, Resources, Writing – original draft, Writing – review & editing. **Bart J.H. van Stratum:** Data curation, Resources, Writing – review & editing. **Iolanda Ialongo:** Investigation, Writing – original draft, Writing – review & editing. **Frédéric Chevallier:** Methodology, Writing – review & editing. **Johanna Tamminen:** Supervision, Writing – review & editing. **Dominik Brunner:** Supervision, Writing – review & editing, Investigation. **Grégoire Broquet:** Supervision, Writing – review & editing.

Declaration of competing interest

The authors declare that they have no known competing financial interests or personal relationships that could have appeared to influence the work reported in this paper.

Data availability

MicroHH columns created in EU H2020 project CoCO2 are available online at https://doi.org/10.5281/zenodo.7448143 (Koene and Brunner, 2023). The Copernicus Sentinel-5P/TROPOMI data used in this study can be accessed from the S5P-PAL system https://data-portal.s5p-pal.com/.

Acknowledgments

Most of the work performed in this paper was done in the framework of EU H2020 project CoCO2 (Grant No. 958927). The FMI team also acknowledge additional funding from the Research Council of Finland (Grant Numbers 353082, 357904, 359196, 359455 and 331829). The Copernicus Sentinel-5P/TROPOMI data used in this work are provided as part of the Sentinel-5P Product Algorithm Laboratory (S5P-PAL).

Appendix A. Supplementary data

Supplementary material related to this article can be found online at https://doi.org/10.1016/j.apr.2024.102171.

References

Bange, P., Janssen, L., Nieuwstadt, F., Visser, H., Erbrink, J., 1991. Improvement of the modelling of daytime nitrogen oxide oxidation in plumes by using instantaneous plume dispersion parameters. Atmos. Environ. A 25 (10), 2321–2328. http://dx.doi.org/10.1016/0960-1686(91)90106-H.

Beirle, S., Boersma, K.F., Platt, U., Lawrence, M.G., Wagner, T., 2011. Megacity emissions and lifetimes of nitrogen oxides probed from space. Science 333 (6050), 1737–1739. http://dx.doi.org/10.1126/science.1207824.

Beirle, S., Borger, C., Dörner, S., Eskes, H., Kumar, V., de Laat, A., Wagner, T., 2021. Catalog of NO_x emissions from point sources as derived from the divergence of the NO_2 flux for TROPOMI. Earth Syst. Sci. Data 13 (6), 2995–3012. http://dx.doi.org/10.5194/essd-13-2995-2021.

Beirle, S., Borger, C., Dörner, S., Li, A., Hu, Z., Liu, F., Wang, Y., Wagner, T., 2019. Pinpointing nitrogen oxide emissions from space. Sci. Adv. 5 (11), http://dx.doi.org/10.1126/sciadv.aax9800.

Beirle, S., Borger, C., Jost, A., Wagner, T., 2023. Improved catalog of NO_x point source emissions (version 2). Earth Syst. Sci. Data 15 (7), 3051–3073. http://dx.doi.org/10.5194/essd-15-3051-2023.

Bovensmann, H., Buchwitz, M., Burrows, J.P., Reuter, M., Krings, T., Gerilowski, K., Schneising, O., Heymann, J., Tretner, A., Erzinger, J., 2010. A remote sensing technique for global monitoring of power plant CO_2 emissions from space and related applications. Atmos. Meas. Tech. 3 (4), 781–811. http://dx.doi.org/10.5194/amt-3-781-2010.

Brunner, D., Kuhlmann, G., Marshall, J., Clément, V., Fuhrer, O., Broquet, G., Löscher, A., Meijer, Y., 2019. Accounting for the vertical distribution of emissions in atmospheric CO_2 simulations. Atmos. Chem. Phys. 19 (7), 4541–4559. http://dx.doi.org/10.5194/acp-19-4541-2019.

Castellanos, P., Boersma, K., 2012. Reductions in nitrogen oxides over Europe driven by environmental policy and economic recession. Sci. Rep. 2, 265. http://dx.doi.org/10.1038/srep00265.

Chevallier, F., Broquet, G., Zheng, B., Ciais, P., Eldering, A., 2022. Large CO_2 emitters as seen from satellite: Comparison to a gridded global emission inventory. Geophys. Res. Lett. 49 (5), http://dx.doi.org/10.1029/2021GL097540, e2021GL097540, e2021GL097540 2021GL097540.

Damian, V., Sandu, A., Damian, M., Potra, F., Carmichael, G.R., 2002. The kinetic preprocessor KPP-a software environment for solving chemical kinetics. Comput. Chem. Eng. 26 (11), 1567–1579. http://dx.doi.org/10.1016/S0098-1354(02)00128-X.

de Foy, B., Lu, Z., Streets, D.G., 2016. Impacts of control strategies, the great recession and weekday variations on NO_2 columns above North American cities. Atmos. Environ. 138, 74–86.

de Foy, B., Lu, Z., Streets, D.G., Lamsal, L.N., Duncan, B.N., 2015. Estimates of power plant NO_x emissions and lifetimes from OMI NO_2 satellite retrievals. Atmos. Environ. 116, 1–11.

de Foy, B., Schauer, J.J., 2022. An improved understanding of NO_x emissions in South Asian megacities using TROPOMI NO_2 retrievals. Environ. Res. Lett. 17 (2), 024006. http://dx.doi.org/10.1088/1748-9326/ac48b4.

de Foy, B., Wilkins, J.L., Lu, Z., Streets, D.G., Duncan, B.N., 2014. Model evaluation of methods for estimating surface emissions and chemical lifetimes from satellite data. Atmos. Environ. 98, 66–77. http://dx.doi.org/10.1016/j.atmosenv.2014.08.051.

Frankenberg, C., Thorpe, A.K., Thompson, D.R., Hulley, G., Kort, E.A., Vance, N., Borchardt, J., Krings, T., Gerilowski, K., Sweeney, C., Conley, S., Bue, B.D., Aubrey, A.D., Hook, S., Green, R.O., 2016. Airborne methane remote measurements reveal heavy-tail flux distribution in four corners region. Proc. Natl. Acad. Sci. 113 (35), 9734–9739. http://dx.doi.org/10.1073/pnas.1605617113.

Goldberg, D.L., Harkey, M., de Foy, B., Judd, L., Johnson, J., Yarwood, G., Holloway, T., 2022. Evaluating NO_x emissions and their effect on o_3 production in Texas using TROPOMI NO_2 and HCHO. Atmos. Chem. Phys. 22 (16), 10875–10900. http://dx.doi.org/10.5194/acp-22-10875-2022.

Hakkarainen, J., Ialongo, I., Koene, E., Szeląg, M., Tamminen, J., Kuhlmann, G., Brunner, D., 2022. Analyzing local carbon dioxide and nitrogen oxide emissions from space using the divergence method: An application to the synthetic smartcarb dataset. Front. Remote Sen. 3, http://dx.doi.org/10.3389/frsen.2022.878731.

Hakkarainen, J., Ialongo, I., Oda, T., Szeląg, M.E., O'Dell, C.W., Eldering, A., Crisp, D., 2023a. Building a bridge: Characterizing major anthropogenic point sources in the South African highveld region using OCO-3 carbon dioxide snapshot area maps and sentinel-5P/TROPOMI nitrogen dioxide columns. Environ. Res. Lett. 18 (3), 035003. http://dx.doi.org/10.1088/1748-9326/acb837.

Hakkarainen, J., Szeląg, M.E., Ialongo, I., Retscher, C., Oda, T., Crisp, D., 2021. Analyzing nitrogen oxides to carbon dioxide emission ratios from space: A case study of matimba power station in South Africa. Atmos. Environ. X 10, 100110. http://dx.doi.org/10.1016/j.aeaoa.2021.100110.

Hakkarainen, J., et al., 2023b. Benchmarking of Plume Detection and Quantification Methods. Technical Report, FMI, URL https://www.coco2-project.eu/node/366, CoCO2: Prototype system for a Copernicus CO_2 service.

Hanrahan, P.L., 1999. The plume volume molar ratio method for determining NO_2/NO_x ratios in modeling-part II: Evaluation studies. J. Air Waste Manage. Assoc. 49 (11), 1332–1338. http://dx.doi.org/10.1080/10473289.1999.10463961.

van Heerwaarden, C.C., van Stratum, B.J.H., Heus, T., Gibbs, J.A., Fedorovich, E., Mellado, J.P., 2017. Microhh 1.0: A computational fluid dynamics code for direct numerical simulation and large-eddy simulation of atmospheric boundary layer flows. Geosci. Model Dev. 10 (8), 3145–3165. http://dx.doi.org/10.5194/gmd-10-3145-2017.

Huijnen, V., Flemming, J., Chabrillat, S., Errera, Q., Christophe, Y., Blechschmidt, A.-M., Richter, A., Eskes, H., 2016. C-IFS-CB05-BASCOE: Stratospheric chemistry in the integrated forecasting system of ECMWF. Geosci. Model Dev. 9 (9), 3071–3091. http://dx.doi.org/10.5194/gmd-9-3071-2016.

Inness, A., Ades, M., Agustí-Panareda, A., Barré, J., Benedictow, A., Blechschmidt, A.-M., Dominguez, J.J., Engelen, R., Eskes, H., Flemming, J., Huijnen, V., Jones, L., Kipling, Z., Massart, S., Parrington, M., Peuch, V.-H., Razinger, M., Remy, S., Schulz, M., Suttie, M., 2019. The CAMS reanalysis of atmospheric composition. Atmos. Chem. Phys. 19 (6), 3515–3556. http://dx.doi.org/10.5194/acp-19-3515-2019.

Ionov, D.V., Makarova, M.V., Kostsov, V.S., Foka, S.C., 2022. Assessment of the NO_x integral emission from the st.petersburg megacity by means of mobile DOAS measurements combined with dispersion modelling. Atmos. Pollut. Res. 13 (12), 101598. http://dx.doi.org/10.1016/j.apr.2022.101598.

Janssen, L.H.J.M., 1988. Reactions of Nitrogen Oxides in Power-Plant Plumes: models and Measurements (Ph.D. thesis). TU Delft, Available at http://resolver.tudelft.nl/uuid:0e279714-5347-4e32-8c84-e29e86644532.

Koene, E., Brunner, D., 2022. CoCO2 WP4.1 library of plumes (1.0) [data set]. http://dx.doi.org/10.5281/zenodo.7448144.

Koene, E., Brunner, D., 2023. Assessment of Plume Model Performance. Technical Report, Empa, URL https://www.coco2-project.eu/node/357, CoCO2: Prototype system for a Copernicus CO_2 service.

Krol, M., van Stratum, B., Anglou, I., Boersma, K.F., 2024. Estimating NO_x emissions of stack plumes using a high-resolution atmospheric chemistry model and satellite-derived NO_2 columns. EGUsphere 2024, 1–32. http://dx.doi.org/10.5194/egusphere-2023-2519.

Kuhlmann, G., Brunner, D., Broquet, G., Meijer, Y., 2020. Quantifying CO_2 emissions of a city with the Copernicus anthropogenic CO_2 monitoring satellite mission. Atmos. Meas. Tech. 13 (12), 6733–6754. http://dx.doi.org/10.5194/amt-13-6733-2020.

Kuhlmann, G., Henne, S., Meijer, Y., Brunner, D., 2021. Quantifying CO_2 emissions of power plants with CO_2 and NO_2 imaging satellites. Frontiers in Remote Sensing 2, 14. http://dx.doi.org/10.3389/frsen.2021.689838.

Kuhlmann, G., Koene, E.F., Meier, S., Brunner, D., Santaren, D., Broquet, G., Chevallier, F., Hakkarainen, J., Nurmela, J., Amorós, L., Tamminen, J., 2024. The *ddeq* Python library for point source quantification from remote sensing images (version 1.0). EGUsphere http://dx.doi.org/10.5194/egusphere-2023-2936, [preprint].

Levelt, P.F., Joiner, J., Tamminen, J., Veefkind, J.P., Bhartia, P.K., Stein Zweers, D.C., Duncan, B.N., Streets, D.G., Eskes, H., van der A, R., McLinden, C., Fioletov, V., Carn, S., de Laat, J., DeLand, M., Marchenko, S., McPeters, R., Ziemke, J., Fu, D., Liu, X., Pickering, K., Apituley, A., González Abad, G., Arola, A., Boersma, F., Chan Miller, C., Chance, K., de Graaf, M., Hakkarainen, J., Hassinen, S., Ialongo, I., Kleipool, Q., Krotkov, N., Li, C., Lamsal, L., Newman, P., Nowlan, C., Suleiman, R., Tilstra, L.G., Torres, O., Wang, H., Wargan, K., 2018. The ozone monitoring instrument: Overview of 14 years in space. Atmos. Chem. Phys. 18 (8), 5699–5745. http://dx.doi.org/10.5194/acp-18-5699-2018.

Lorente, A., Boersma, K.F., Eskes, H.J., Veefkind, J.P., van Geffen, J.H.G.M., de Zeeuw, M.B., Denier van der Gon, H.A.C., Beirle, S., Krol, M.C., 2019. Quantification of nitrogen oxides emissions from build-up of pollution over Paris with TROPOMI. Sci. Rep. 9 (1), 20033. http://dx.doi.org/10.1038/s41598-019-56428-5.

Madronich, S., Flocke, S., 1999. The role of solar radiation in atmospheric chemistry. In: Boule, P. (Ed.), Environmental Photochemistry. Springer Berlin Heidelberg, Berlin, Heidelberg, pp. 1–26. http://dx.doi.org/10.1007/978-3-540-69044-3_1.

Meijer, Y., et al., 2020. Copernicus CO_2 Monitoring Mission Requirements Document. Technical Report, European Space Agency, URL https://esamultimedia.esa.int/docs/EarthObservation/CO2M_MRD_v3.0_20201001_Issued.pdf, Issue 3.0, EOP-SM/3088/YM-ym.

Merlaud, A., Belegante, L., Constantin, D.-E., Den Hoed, M., Meier, A.C., Allaart, M., Ardelean, M., Arseni, M., Bösch, T., Brenot, H., Calcan, A., Dekemper, E., Donner, S., Dörner, S., Balanica Dragomir, M.C., Georgescu, L., Nemuc, A., Nicolae, D., Pinardi, G., Richter, A., Rosu, A., Ruhtz, T., Schönhardt, A., Schuettemeyer, D., Shaiganfar, R., Stebel, K., Tack, F., Nicolae Vâjâiac, S., Vasilescu, J., Vanhamel, J., Wagner, T., Van Roozendael, M., 2020. Satellite validation strategy assessments based on the AROMAT campaigns. Atmos. Meas. Tech. 13 (10), 5513–5535. http://dx.doi.org/10.5194/amt-13-5513-2020.

Nassar, R., Hill, T.G., McLinden, C.A., Wunch, D., Jones, D.B.A., Crisp, D., 2017. Quantifying CO_2 emissions from individual power plants from space. Geophys. Res. Lett. 44 (19), 10,045–10,053. http://dx.doi.org/10.1002/2017GL074702.

Neggers, R.A.J., Siebesma, A.P., Heus, T., 2012. Continuous single-column model evaluation at a permanent meteorological supersite. Bull. Am. Meteorol. Soc. 93 (9), 1389–1400. http://dx.doi.org/10.1175/BAMS-D-11-00162.1.

Potts, D.A., Timmis, R., Ferranti, E.J.S., Vande Hey, J.D., 2022. Identifying and accounting for the Coriolis effect in satellite NO_2 observations and emission estimates. Atmos. Chem. Phys. Discuss. 2022, 1–20. http://dx.doi.org/10.5194/acp-2022-599.

Razňjević, A., 2023. High-Resolution Modelling of Plume Dispersion (Ph.D. thesis). Wageningen University, Available at https://doi.org/10.18174/634327.

Reuter, M., Buchwitz, M., Hilboll, A., Richter, A., Schneising, O., Hilker, M., Heymann, J., Bovensmann, H., Burrows, J.P., 2014. Decreasing emissions of NO_x relative to CO_2 in East Asia inferred from satellite observations. Nat. Geosci. 7 (11), 792–795. http://dx.doi.org/10.1038/ngeo2257.

Reuter, M., Buchwitz, M., Schneising, O., Krautwurst, S., O'Dell, C.W., Richter, A., Bovensmann, H., Burrows, J.P., 2019. Towards monitoring localized CO_2 emissions from space: Co-located regional CO_2 and NO_2 enhancements observed by the OCO-2 and S5p satellites. Atmos. Chem. Phys. 19 (14), 9371–9383. http://dx.doi.org/10.5194/acp-19-9371-2019.

Rey-Pommier, A., Chevallier, F., Ciais, P., Broquet, G., Christoudias, T., Kushta, J., Hauglustaine, D., Sciare, J., 2022. Quantifying NO_x emissions in Egypt using TROPOMI observations. Atmos. Chem. Phys. 22 (17), 11505–11527. http://dx.doi.org/10.5194/acp-22-11505-2022.

Sandu, A., Sander, R., Long, M.S., Yantosca, R.M., Lin, H., Shen, L., Jacob, D.J., 2022. KineticPreProcessor/KPP: the kinetic PreProcessor (KPP) 3.0.0. http://dx.doi.org/10.5281/zenodo.7308373.

Santaren, D., Hakkarainen, J., Kuhlmann, G., Koene, E., Chevallier, F., Ialongo, I., Lindqvist, H., Nurmela, J., Tamminen, J., Amoros, L., Broquet, G., 2024. Benchmarking data-driven inversion methods for the estimation of local CO_2 emissions from XCO_2 and NO_2 satellite images. Atmos. Meas. Tech. Discuss. http://dx.doi.org/10.5194/amt-2023-241, [preprint].

Schwaerzel, M., Emde, C., Brunner, D., Morales, R., Wagner, T., Berne, A., Buchmann, B., Kuhlmann, G., 2020. Three-dimensional radiative transfer effects on airborne and ground-based trace gas remote sensing. Atmos. Meas. Tech. 13 (8), 4277–4293. http://dx.doi.org/10.5194/amt-13-4277-2020, URL https://amt.copernicus.org/articles/13/4277/2020/.

Seinfeld, J., Pandis, S., 2006. Atmospheric Chemistry and Physics: From Air Pollution to Climate Change. 2nd Edition. John Wiley & Sons, New York.

Shaiganfar, R., Beirle, S., Denier van der Gon, H., Jonkers, S., Kuenen, J., Petetin, H., Zhang, Q., Beekmann, M., Wagner, T., 2017. Estimation of the Paris NO_x emissions from mobile MAX-doas observations and CHIMERE model simulations during the MEGAPOLI campaign using the closed integral method. Atmos. Chem. Phys. 17 (12), 7853–7890. http://dx.doi.org/10.5194/acp-17-7853-2017.

van Stratum, B.J.H., van Heerwaarden, C.C., de Arellano, J.V.-G., 2023. The benefits and challenges of downscaling a global reanalysis with doubly-periodic large-eddy simulations. Authorea http://dx.doi.org/10.22541/essoar.168167362.25141062/v1, preprint submtitted to JAMES.

Varon, D.J., McKeever, J., Jervis, D., Maasakkers, J.D., Pandey, S., Houweling, S., Aben, I., Scarpelli, T., Jacob, D.J., 2019. Satellite discovery of anomalously large methane point sources from oil/gas production. Geophys. Res. Lett. 46 (22), 13507–13516. http://dx.doi.org/10.1029/2019GL083798.

Veefkind, J., Aben, I., McMullan, K., Förster, H., de Vries, J., Otter, G., Claas, J., Eskes, H., de Haan, J., Kleipool, Q., van Weele, M., Hasekamp, O., Hoogeveen, R., Landgraf, J., Snel, R., Tol, P., Ingmann, P., Voors, R., Kruizinga, B., Vink, R., Visser, H., Levelt, P., 2012. TROPOMI on the ESA sentinel-5 precursor: A GMES mission for global observations of the atmospheric composition for climate, air quality and ozone layer applications. Remote Sens. Environ. 120, 70–83. http://dx.doi.org/10.1016/j.rse.2011.09.027, The Sentinel Missions - New Opportunities for Science.

Vilà-Guerau de Arellano, J., Talmon, A.M., Builtjes, P.J., 1990. A chemically reactive plume model for the NO-NO_2-o_3 system. Atmos. Environ. A 24 (8), 2237–2246. http://dx.doi.org/10.1016/0960-1686(90)90255-L, Proceedings of the 2nd International Conference on Atmospheric Sciences and Application to Air Quality.

Wagner, T., Warnach, S., Beirle, S., Bobrowski, N., Jost, A., Puķīte, J., Theys, N., 2023. Investigation of three-dimensional radiative transfer effects for UV–Vis satellite and ground-based observations of volcanic plumes. Atmos. Meas. Tech. 16 (6), 1609–1662. http://dx.doi.org/10.5194/amt-16-1609-2023.

Zhang, Q., Boersma, K.F., Zhao, B., Eskes, H., Chen, C., Zheng, H., Zhang, X., 2023. Quantifying daily NO_x and CO_2 emissions from Wuhan using satellite observations from TROPOMI and OCO-2. Atmos. Chem. Phys. 23 (1), 551–563. http://dx.doi.org/10.5194/acp-23-551-2023.

Zheng, B., Chevallier, F., Ciais, P., Broquet, G., Wang, Y., Lian, J., Zhao, Y., 2020. Observing carbon dioxide emissions over China's cities and industrial areas with the orbiting carbon observatory-2. Atmos. Chem. Phys. 20 (14), 8501–8510. http://dx.doi.org/10.5194/acp-20-8501-2020.